Available online at www.sciencedirect.com
SCIENCE DIRECT®
Journal of Sound and Vibration 290 (2006) 290–308
JOURNAL OF SOUND AND VIBRATION
www.elsevier.com/locate/jsvi

# Higher-order rod approximations for the propagation of longitudinal stress waves in elastic bars

Simon P. Anderson*

*School of Mechanical, Aerospace and Civil Engineering, University of Manchester, P.O. Box 88, Manchester M60 1QD, UK*

Received 1 April 2004; received in revised form 30 March 2005; accepted 31 March 2005
Available online 19 August 2005

**Abstract**

The elementary one-dimensional wave theory is often used to describe the propagation of longitudinal stress waves along a slender bar. However, for relatively large diameter bars and high-frequency waves, geometrical wave dispersion due to lateral inertia occurs, rendering this single-mode theory inaccurate. In this paper, an approximate four-mode rod equation for a circular bar that takes wave dispersion into account is presented. Little difference is observed between the dispersion curves of the four-mode equation and the Pochhammer–Chree equation that gives the exact propagation coefficient for an infinite circular bar. The advantage of the former is that its solution can be computed directly whereas the latter requires an iterative procedure. Also presented are different orders of rod approximation equations derived from the Pochhammer equation, each of which can also be solved directly. Applications of the more accurate rod equations include correcting for wave dispersion in a split Hopkinson pressure bar (SHPB) test, and more accurately determining the frequency-dependent elastic modulus of a viscoelastic bar from an experimentally measured propagation coefficient.


## 1. Introduction

In impact engineering it is often required to accurately predict the propagation of longitudinal stress waves along a slender bar. A classic example is the split Hopkinson pressure bar (SHPB)

*Fax: +44 161 200 3849.
*E-mail address:* simon.anderson@postgrad.manchester.ac.uk.

0022-460X/$ - see front matter © 2005 Elsevier Ltd. All rights reserved.
doi:10.1016/j.jsv.2005.03.031

apparatus. The SHPB is indespensable for determining the dynamic properties of materials. Essentially it consists of the specimen to be tested placed between an input and an output bar, both of which are instrumented with strain gauges. The input bar is impacted with a striker resulting in an incident stress wave propagating through the bar. At the bar–specimen interface, part of the incident wave is reflected back into the input bar while the remaining wave is transmitted through the output bar. The normal force and displacement at the proximal end of the specimen is determined from the incident and reflected strain waves in the input bar. For the two strains to be measured separately (i.e., for no wave overlap to occur), the measurements are taken at the centre of the bar and shifted in time to the end of the bar, thus effectively using the elementary one-dimensional wave theory. This procedure is fine when the effects of wave dispersion and attenuation are minimal. This is true in the case of an elastic medium of propagation, and either relatively low-frequency waves or a small diameter bar. However, when the frequency of the disturbance is high, such as in high strain-rate loading, or the diameter of the bar is relatively large, the effects of lateral inertia become significant. This leads to geometrical wave dispersion.

It is well known that when testing low impedance specimens such as cellular solids, the use of low impedance bars, such as polymer bars, is preferable. However, due to the rheological properties of these viscoelastic bars, material wave dispersion and attenuation occurs [1]. A further issue is that since there is a practical limitation on how small cellular solid specimens can be made, and due to the lower elastic modulus of polymer bars compared to elastic bars, the viscoelastic SHPB set-up often requires larger diameter bars [2]. Therefore, geometrical dispersion also occurs.

In both of the above cases the elementary wave theory cannot accurately predict the propagation of stress waves along the bar. The exact propagation in a circular bar of infinite length can be described by the Pochhammer–Chree equation. This equation can still be used with sufficient accuracy for long finite bars [3]. However, the disadvantages of using the Pochhammer equation are that it cannot be solved directly and it is only applicable to bars of circular cross-section. Green [4] provided a review of several approximate rod theories for longitudinal wave propagation with varying levels of success. In this paper a four-mode rod equation is presented that is comparable to the Pochhammer equation in terms of the accuracy of the dominant propagating mode, without suffering from its limitations. The four-mode equation is derived for a circular bar, however since the procedure is based on approximating two-dimensional displacement fields through the bar, similar equations can be derived for other simple cross-sections. Also presented are different orders of approximation to the Pochhammer equation, all of which can also be solved directly.

In computing normal forces in the viscoelastic SHPB set-up, the elastic modulus of the bars employed need to be known accurately. In contrast to elastic materials, the elastic modulus of viscoelastic materials is frequency-dependent, due to the damping brought about by internal viscosity [1]. As a result, the elastic modulus obtained from a static test can no longer be used in dynamic experiments. The problem increases when it is recognised that the mechanical properties of a viscoelastic rod may also vary slightly with the extrusion process [5]. A standard curve of elastic modulus against frequency would then become inaccurate. This can be overcome by determining the complex elastic modulus of each rod experimentally. Bacon [5] demonstrated an experimental method to determine the propagation coefficient of a viscoelastic rod by making use

of a single strain measurement along a bar. By applying this method it is possible to rearrange the approximate rod equations and thus determine the complex elastic modulus. Compared to computing the propagation coefficient, the same percentage error occurs at a lower frequency when determining the complex elastic modulus. For this purpose the elementary theory is therefore limited to even smaller diameter bars and lower-frequency waves. The four-mode equation is again shown to be an extremely good approximation in comparison to the true elastic modulus. Use of the more accurate rod approximation in the viscoelastic SHPB set-up would allow the conditions at the end of the bars to be more accurately evaluated, thus providing a better understanding of the specimens being tested.

The paper is arranged as follows: in Section 2 the four-mode equation and the Pochhammer approximation equations are developed; Section 3 compares the accuracies of the rod equations for determining both the phase velocity of an aluminium bar, and the elastic modulus from the exact propagation coefficient; finally, Section 4 concludes the paper. In the equations to follow, it is valid for all the material properties to be a function of frequency, despite the omission of their dependency. The equations are therefore applicable to viscoelastic solids.

## 2. Rod theories

### 2.1. Single-mode equations

In brief, the elementary wave theory assumes deformation only takes place in the axial direction, and that the deformed planes remain parallel to the undeformed planes. Thus, it is a single-mode theory since only 1dof in the possible deformation is present. This leads to the following governing equation of motion:

$$\frac{\partial^2 u}{\partial x^2} = \frac{1}{E/\rho}\frac{\partial^2 u}{\partial t^2}, \tag{1}$$

where $u = u(x,t)$ is the single function describing the axial displacement, $x$ is the axial distance along the bar, $t$ is time, and $E$ and $\rho$ are the elastic modulus and mass density of the bar, respectively. For an elastic material, $\sqrt{E/\rho} = c_0$ is the constant elementary longitudinal phase velocity. Firstly, assume a harmonic solution of the form

$$u(x,t) = \sum_{\omega} \tilde{u}(x,\omega)\mathrm{e}^{\gamma x + \mathrm{i}\omega t}, \tag{2}$$

where $\omega$ is circular frequency, i is the imaginary unit, and $\gamma = \gamma(\omega)$ is the propagation coefficient of the bar and is defined as

$$\gamma(\omega) = \alpha(\omega) + \mathrm{i}k(\omega),$$

where $\alpha(\omega)$ and $k(\omega)$ are the attenuation coefficient and wavenumber, respectively. Substituting Eq. (2) into Eq. (1) leads to the following solution for $\gamma^2$:

$$\gamma^2 = -\frac{\rho\omega^2}{E}.$$

As the lateral dimensions of the bar increases, or the frequency of the propagating wave increases, the effects of lateral inertia become significant, which leads to erroneous results in the elementary theory.

The Love theory extends the elementary theory by taking into account the energy that goes into lateral deformation. The governing equation of motion thus becomes [6]

$$\frac{\partial^2 u}{\partial x^2} + \frac{v^2 \rho J}{EA} \frac{\partial^4 u}{\partial x^2 \partial t^2} = \frac{1}{E/\rho} \frac{\partial^2 u}{\partial t^2},$$

where $v$ and $J$ are Poisson's ratio and second polar moment of area, respectively. Following the same procedure as before, the propagation coefficient for a rod of circular cross-section is

$$\gamma^2 = -\frac{\rho\omega^2}{E - \rho a^2 \omega^2 v^2/2},$$

where $a$ is the radius of the bar. This obviously reduces to the elementary theory when $a = 0$ or $v = 0$, corresponding to suppressed lateral effects.

### 2.2. Multimode equations

A more accurate description of the rod deformation can be obtained by increasing the number of possible deformation modes (i.e., dof of the deformation). The functions describing the exact displacement fields through the cross-section of a rod can be expressed as an infinite series of orthogonal polynomials [7]. For a circular rod it is convenient to employ cylindrical coordinates to describe the axial and radial displacements, noting that from symmetry the circumferential displacement is zero. Mindlin and McNiven [8] represented these displacements in terms of the classical Jacobi polynomial, such that

$$u_x(x, r, t) = \sum_{n=0}^{\infty} \mathscr{U}_n(r) u_n(x, t), \tag{3a}$$

$$u_r(x, r, t) = \sum_{n=0}^{\infty} \mathscr{V}_n(r) v_n(x, t), \tag{3b}$$

$$u_\theta(x, r, t) = 0, \tag{3c}$$

where $u_x$, $u_r$ and $u_\theta$ are the axial, radial and circumferential displacements, respectively, $u_n$ and $v_n$ are the coefficients in the series expansions, $n$ is the mode number and $r$ is the radial distance from the neutral axis. The orthogonal polynomials defined over the interval $[0, a]$ are

$$\mathscr{U}_n(r) = \sum_{k=0}^{n} (-1)^k \binom{n}{k} \frac{(n+1)^{(k)}}{k!} \left(\frac{r}{a}\right)^{2k}, \tag{4a}$$

$$\mathscr{V}_n(r) = \sum_{k=0}^{n} (-1)^k \binom{n}{k} \frac{(n+k)^{(k)}}{(k+1)!} \left(\frac{r}{a}\right)^{2k+1}, \tag{4b}$$

where

$$n! = \begin{cases} n(n-1)\cdots 1 & \text{when} \quad n \neq 0, \\ 1 & \text{when} \quad n = 0, \end{cases}$$

$$n^{(k)} = \begin{cases} n(n+1)\cdots(n+k-1) & \text{when} \quad k \neq 0, \\ 1 & \text{when} \quad k = 0, \end{cases}$$

$$\binom{n}{k} = \frac{n!}{k!(n-k)!},$$

are factorial, rising factoring, and the binomial coefficient, respectively. By representing the displacements in this way, the following favourable properties can be made use of in deriving the multimode equations of motion [8]

$$\int_0^a r\mathscr{U}_n(r)\mathscr{U}_m(r)\,\mathrm{d}r = \frac{a^2}{2(2n+1)}\,\delta_{nm}, \tag{5a}$$

$$\int_0^a r\mathscr{V}_n(r)\mathscr{V}_m(r)\,\mathrm{d}r = \frac{a^2}{4(n+1)^3}\,\delta_{nm}, \tag{5b}$$

where $\delta_{nm}$ is the Kronecker delta defined as

$$\delta_{nm} = \begin{cases} 1 & \text{when} \quad n = m, \\ 0 & \text{when} \quad n \neq m. \end{cases}$$

The first two polynomials of each series, which describe the possible deformation modes, can be expressed as

$$\mathscr{U}_0(r) = 1, \tag{6a}$$

$$\mathscr{U}_1(r) = 1 - \frac{2r^2}{a^2}, \tag{6b}$$

$$\mathscr{V}_0(r) = \frac{r}{a}, \tag{6c}$$

$$\mathscr{V}_1(r) = \frac{r}{a} - \frac{3r^3}{2a^3}. \tag{6d}$$

These deformation modes are depicted in Fig. 1. As the mode number increases, the accuracy of the approximate displacement profile improves. Note that when deriving the higher-order rod equations, the lower-order terms are still included, thus increasing the number of deformation dof in the rod.

It is easy to see that the elementary theory only uses $\mathscr{U}_0$ in approximating the deformation. The Mindlin–Herrmann rod equation [9] considers radial deformation by including $\mathscr{V}_0$ in the derivation, therefore making it a two-mode theory. This leads to solving a quadratic equation in $\gamma^2$. For such multimode rod equations, including the Pochhammer equation, only one of the

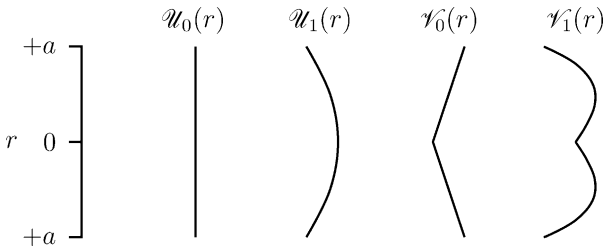


Fig. 1. First two axial and radial deformation modes based on the Jacobi polynomials.

solutions that corresponds to the first (i.e., dominant) propagating mode is of any real significance at typical testing frequencies [3], and is therefore the only mode of interest here. Mindlin and McNiven [8] further added the second axial term, namely $\mathscr{U}_1$, and presented a more accurate three-mode theory. In this case the propagation coefficient is obtained by solving a cubic in $\gamma^2$.

In the following section, a four-mode rod equation for a circular rod is presented by describing the displacement through the cross-section of the rod in terms of the first two axial and radial deformation modes given by Eq. (6). Compared to the three-mode rod equation this derivation includes the second radial term, $\mathscr{V}_1$. The motivation for extending the previous rod equations to four modes is that this will inevitably lead to the higher-order quartic (or biquadratic) equation in $\gamma^2$, which may improve on the accuracy of the three-mode equation. The solutions to such equations can be determined directly in terms of a finite algebraic expression using the relatively simple quartic formula. However, according to the Abel–Ruffini theorem, the roots of polynomials of degree greater than four cannot be determined as a finite algebraic expression since they cannot be expressed as a finite number of addition, subtraction, multiplication, division, and root extraction operations [10]. The added complexity in solving these higher-order polynomials may make an iterative method more attractive.

### 2.3. A four-mode rod equation

Omitting the function dependencies for brevity, the displacements in a circular rod are approximated by

$$u_x \approx \mathscr{U}_0 u_0 + \mathscr{U}_1 u_1 = u + \left(1 - \frac{2r^2}{a^2}\right)\phi, \tag{7a}$$

$$u_r \approx \mathscr{V}_0 v_0 + \mathscr{V}_1 v_1 = \frac{r}{a} v + \left(\frac{r}{a} - \frac{3r^3}{2a^3}\right)\psi, \tag{7b}$$

$$u_\theta = 0, \tag{7c}$$

where the displacement variables $u = u(x,t)$, $v = v(x,t)$, $\phi = \phi(x,t)$ and $\psi = \psi(x,t)$ replace the series coefficients $u_0$, $v_0$, $u_1$ and $v_1$, respectively. The corresponding non-zero strains are

$$\varepsilon_{xx} = \frac{\partial u_x}{\partial x}, \tag{8a}$$

$$\varepsilon_{rr} = \frac{\partial u_r}{\partial r}, \tag{8b}$$

$$\varepsilon_{\theta\theta} = \frac{u_r}{r} + \frac{1}{r}\frac{\partial u_\theta}{\partial \theta}, \tag{8c}$$

$$\varepsilon_{xr} = \frac{\partial u_x}{\partial r} + \frac{\partial u_r}{\partial x}. \tag{8d}$$

From the generalised Hooke's law, the stresses in an isotropic solid are given by [11]

$$\sigma_{xx} = \lambda \Delta + 2\mu\varepsilon_{xx}, \tag{9a}$$

$$\sigma_{rr} = \lambda \Delta + 2\mu\varepsilon_{rr}, \tag{9b}$$

$$\sigma_{\theta\theta} = \lambda \Delta + 2\mu\varepsilon_{\theta\theta}, \tag{9c}$$

$$\sigma_{xr} = \mu\varepsilon_{xr}, \tag{9d}$$

where $\Delta = \varepsilon_{xx} + \varepsilon_{rr} + \varepsilon_{\theta\theta}$, and $\mu$ and $\lambda$ are Lamé's constants defined by

$$\mu = \frac{E}{2(1+v)} \quad \text{and} \quad \lambda = \frac{Ev}{(1-2v)(1+v)}. \tag{10}$$

Substituting Eq. (7) into Eq. (8) and then into Eq. (9) leads to the following stress–displacement relationships:

$$\sigma_{xx} = (2\mu + \lambda)\left(\frac{\partial u}{\partial x} + \left(1 - \frac{2r^2}{a^2}\right)\frac{\partial \phi}{\partial x}\right) + \frac{2}{a}\lambda\left(v + \left(1 - \frac{3r^2}{a^2}\right)\psi\right), \tag{11a}$$

$$\sigma_{rr} = \frac{2}{a}(\mu + \lambda)\left(v + \left(1 - \frac{9r^2}{2a^2}\right)\psi\right) + \lambda\left(\frac{\partial u}{\partial x} + \left(1 - \frac{2r^2}{a^2}\right)\frac{\partial \phi}{\partial x} + \frac{3r^2}{a^3}\psi\right), \tag{11b}$$

$$\sigma_{\theta\theta} = \sigma_{rr} + \frac{6\mu r^2}{a^3}\psi, \tag{11c}$$

$$\sigma_{xr} = \frac{\mu}{a}\left(r\frac{\partial v}{\partial x} - \frac{4r}{a}\phi + \left(r - \frac{3r^3}{2a^2}\right)\frac{\partial \psi}{\partial x}\right). \tag{11d}$$

The stress equations of motion of elasticity for the given axisymmetrical problem are [11]

$$\frac{\partial \sigma_{xr}}{\partial r} + \frac{\partial \sigma_{xx}}{\partial x} + \frac{1}{r}\sigma_{xr} = \rho\frac{\partial^2 u_x}{\partial t^2}, \tag{12a}$$

$$\frac{\partial \sigma_{rr}}{\partial r} + \frac{\partial \sigma_{xr}}{\partial x} + \frac{\sigma_{rr} - \sigma_{\theta\theta}}{r} = \rho\frac{\partial^2 u_r}{\partial t^2}. \tag{12b}$$

Observing that for the general case the right-hand side of Eq. (12a) can be written in terms of the orthogonal polynomials as

$$\sum_{n=0}^{\infty} \rho \mathscr{U}_n \frac{\partial^2 u_n}{\partial t^2},$$

which, from property (5), when multiplied by $r\mathscr{U}_m$ and integrated with respect to $r$ results in

$$\frac{1}{2(2m+1)} \rho a^2 \frac{\partial^2 u_m}{\partial t^2}.$$

Similarly, multiplying the right-hand side of Eq. (12b) by $r\mathscr{V}_m$ and integrating with respect to $r$ gives

$$\frac{1}{4(m+1)^3} \rho a^2 \frac{\partial^2 v_m}{\partial t^2}.$$

The significance of this result is that no matter how many modes are included, multiplying the stress equations of motion by the functions $r\mathscr{U}_m$ and $r\mathscr{V}_m$ and integrating over the cross-section leads to an exact right-hand side that contains only one variable, namely $u_m$ and $v_m$, respectively. The equations of motion for $u$ and $\phi$ are obtained by multiplying Eq. (12a) separately by $r$ and $r - 2r^3/a^2$ and integrating over the cross-section, noting that

$$\sigma_{rr} = \sigma_{xr} = 0 \quad \text{when} \quad r = a.$$

Similarly, the equations of motion for $v$ and $\psi$ are obtained by multiplying Eq. (12b) by $r^2/a$ and $r^2/a - 3r^4/2a^3$ and integrating over the cross-section. Thus, the four governing equations of motion are

$$a^2(2\mu+\lambda)\frac{\partial^2 u}{\partial x^2} + 2a\lambda \frac{\partial v}{\partial x} - a\lambda \frac{\partial \psi}{\partial x} = \rho a^2 \frac{\partial^2 u}{\partial t^2}, \tag{13a}$$

$$-4a\lambda \frac{\partial u}{\partial x} + a^2\mu \frac{\partial^2 v}{\partial x^2} - 8(\mu+\lambda)v - 4a\mu \frac{\partial \phi}{\partial x} + 4(\mu+\lambda)\psi = \rho a^2 \frac{\partial^2 v}{\partial t^2}, \tag{13b}$$

$$6a\mu \frac{\partial v}{\partial x} + a^2(2\mu+\lambda)\frac{\partial^2 \phi}{\partial x^2} - 24\mu\phi + 3a\lambda \frac{\partial \psi}{\partial x} = \rho a^2 \frac{\partial^2 \phi}{\partial t^2}, \tag{13c}$$

$$16a\lambda \frac{\partial u}{\partial x} + 32(\mu+\lambda)v - 16a\lambda \frac{\partial \phi}{\partial x} + a^2\mu \frac{\partial^2 \psi}{\partial x^2} - 16(7\mu+4\lambda)\psi = \rho a^2 \frac{\partial^2 \psi}{\partial t^2}. \tag{13d}$$

Again assuming harmonic solutions for $u$, $v$, $\phi$ and $\psi$, and substituting them into Eq. (13), the following simultaneous equation is obtained:

$$\begin{pmatrix} a_{11} & 2a\lambda\gamma & 0 & -a\lambda\gamma \\ & a_{22} & 2a\mu\gamma & -2(\mu+\lambda) \\ & & a_{33} & a\lambda\gamma \\ \text{sym} & & & a_{44} \end{pmatrix} \begin{pmatrix} \tilde{u} \\ \tilde{v} \\ \tilde{\phi} \\ \tilde{\psi} \end{pmatrix} = 0, \tag{14}$$

where the diagonal terms in the symmetric coefficient matrix are given by

$$a_{11} = a^2(2\mu + \lambda)\gamma^2 + \rho a^2\omega^2,$$

$$a_{22} = 4(\mu + \lambda) - \tfrac{1}{2}(a^2\mu\gamma^2 + \rho a^2\omega^2),$$

$$a_{33} = \tfrac{1}{3}(a^2(2\mu + \lambda)\gamma^2 + \rho a^2\omega^2) - 8\mu,$$

$$a_{44} = 7\mu + 4\lambda - \tfrac{1}{16}(a^2\mu\gamma^2 + \rho a^2\omega^2).$$

Equating the determinant of the coefficient matrix to zero gives the characteristic equation for the propagation coefficient, which as expected results in a quartic in $\gamma^2$ given by

$$C_1\gamma^8 + C_2\gamma^6 + C_3\gamma^4 + C_4\gamma^2 + C_5 = 0, \tag{15}$$

where

$$C_1 = a^8\mu^2(2\mu + \lambda)^2,$$

$$C_2 = a^6\mu(2\mu + \lambda)(2\rho a^2\omega^2(3\mu + \lambda) - 24\mu(10\mu + 11\lambda)),$$

$$C_3 = a^4(\rho^2a^4\omega^4(13\mu^2 + 7\mu\lambda + \lambda^2) - 24\rho a^2\omega^2\mu(42\mu^2 + 55\mu\lambda + 14\lambda^2) + 192\mu^2(9\mu + 4\lambda)(2\mu + 3\lambda)),$$

$$C_4 = a^2(2\rho^3a^6\omega^6(3\mu + \lambda) - 24\rho^2a^4\omega^4(28\mu^2 + 26\mu\lambda + 3\lambda^2) + 192\rho a^2\omega^2\mu(47\mu^2 + 62\mu\lambda + 16\lambda^2) - 9216\mu^2(4\mu^2 + 8\mu\lambda + 3\lambda^2)),$$

$$C_5 = \rho a^2\omega^2(\rho a^2\omega^2 - 24\mu)(\rho a^2\omega^2(\rho a^2\omega^2 - 24(5\mu + 3\lambda)) + 384(\mu + \lambda)(2\mu + \lambda)).$$

Eq. (15) may appear complicated, however it can be easily solved directly using the quartic formula (see, for example, Ref. [12]). Note that the governing equations of motion for the elementary, two-mode and three-mode theories can be obtained from Eq. (13) by setting the relevant displacement variables to zero. In the case of the elementary theory, $\nu = 0$ since Poisson's effect is neglected.

### 2.4. The Pochhammer–Chree equation

The exact propagation of stress waves in an infinite rod of circular cross-section can be described by the Pochhammer–Chree equation. For a general rod of either elastic or viscoelastic material, this equation is given by [13]

$$\frac{2\alpha}{a}(\beta^2 - \gamma^2)J_1(\alpha a)J_1(\beta a) - (\beta^2 + \gamma^2)^2J_0(\alpha a)J_1(\beta a) + 4\gamma^2\alpha\beta J_1(\alpha a)J_0(\beta a) = 0, \tag{16}$$

where

$$\alpha^2 = \frac{\rho\omega^2}{2\mu + \lambda} + \gamma^2 \quad \text{and} \quad \beta^2 = \frac{\rho\omega^2}{\mu} + \gamma^2$$

and $J_0$ and $J_1$ are the zero- and first-order Bessel functions of the first kind. Eq. (16) can be expressed more concisely as [14]

$$4\gamma^2\alpha^2\mathscr{J}_1(\beta a) - (\beta^2+\gamma^2)^2\mathscr{J}_1(\alpha a) + 2\alpha^2(\beta^2-\gamma^2) = 0, \tag{17}$$

where

$$\mathscr{J}_1(x) = x\,\frac{J_0(x)}{J_1(x)}, \tag{18}$$

is the modified quotient of Bessel functions of the first kind and was tabulated in Ref. [15]. (The modified quotient will simply be referred to as the Onoe function.) Eq. (16) has to be solved iteratively for the real and imaginary parts of $\gamma$.

### 2.5. Approximating the Pochhammer equation

The zero- and first-order Bessel functions can be expressed as the following infinite series [7]:

$$J_0(x) = \sum_{k=0}^{\infty}\frac{(-1)^k(x/2)^{2k}}{(k!)^2} = 1 - \frac{x^2}{4} + \frac{x^4}{64} - \cdots, \tag{19a}$$

$$J_1(x) = -\frac{\mathrm{d}}{\mathrm{d}x}[J_0(x)] = \frac{x}{2} - \frac{x^3}{16} + \cdots. \tag{19b}$$

By approximating the Bessel functions as finite polynomials of a certain order, and substituting these polynomials into Eq. (16), various levels of approximation for the Pochhammer equation can be obtained. By doing this, comparisons can be made between directly solvable Pochhammer approximations and the deformation mode approximations. For a given approximation order the equations are not expected to be equivalent since one set of equations contains the approximation in the Bessel functions and the other in the displacement field.

Probably the easiest method to derive the approximations is by obtaining the series expansion for the Onoe function and subsequently using Eq. (17). This can be achieved in the following manner:

$$\begin{aligned}(2/x)J_1(x) &= \sum_{k=0}^{\infty}\frac{(-1)^k(x/2)^{2k}}{k!(k+1)!}\\ &= 1 - \sum_{k=1}^{\infty}\frac{(-1)^{k+1}(x/2)^{2k}}{k!(k+1)!}\\ &= 1 - z,\end{aligned}$$

where

$$z = \sum_{k=1}^{\infty}\frac{(-1)^{k+1}(x/2)^{2k}}{k!(k+1)!}. \tag{20}$$

By making use of the negative binomial series, which is given by

$$(1-z)^{-1} = 1 + z + z^2 + z^3 + \cdots \quad \text{if} \quad |z|<1,$$

it follows that

$$[(2/x)J_1(x)]^{-1} = \sum_{m=0}^{\infty} \left( \sum_{k=1}^{\infty} \frac{(-1)^{k+1}(x/2)^{2k}}{k!(k+1)!} \right)^m .$$

Thus the Onoe expansion series and the terms up to and including the fourth-order are given by

$$\begin{aligned} \mathscr{J}_1(x) &= 2J_0(x)[(2/x)J_1(x)]^{-1} \\ &= 2\sum_{k=0}^{\infty} \frac{(-1)^k(x/2)^{2k}}{(k!)^2} \cdot \sum_{m=0}^{\infty} \left( \sum_{k=1}^{\infty} \frac{(-1)^{k+1}(x/2)^{2k}}{k!(k+1)!} \right)^m \\ &= 2 - \frac{x^2}{4} - \frac{x^4}{96} - \frac{x^6}{1536} - \frac{x^8}{23\,040} - \cdots . \end{aligned} \tag{21}$$

It is easy to verify that substituting only the first term of this expansion into Eq. (17), corresponding to the zero-order approximation, reduces the exact equation to the elementary theory.

The negative binomial series will only converge if $|z|<1$, and so in order to test the applicability of the series expansion presented above, Fig. 2 shows the variation of $|z|$ with $x$. It is clear that the expansion series does not converge for all values of $x$, however provided $x<x_c \approx 3.83$ then the expansion series is valid. However, since the series is to be approximated by truncation, the main concern is the increase in the truncation error as $x$ increases, and not the convergence of the series.

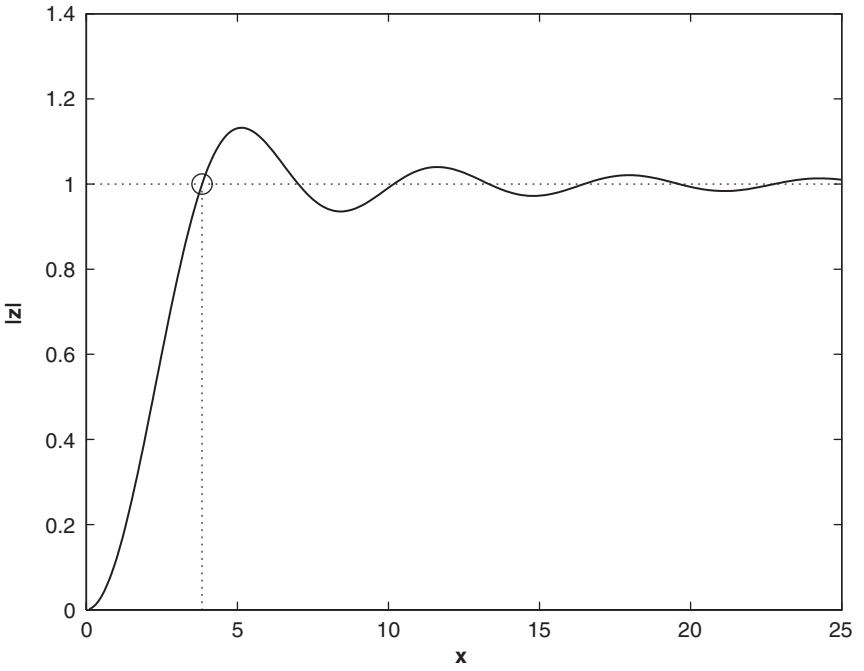


Fig. 2. Applicability of the expansion series for the Onoe function.

The reason for the breakdown at $x_c$ is that there are an infinite number of discontinuities in $\mathscr{J}_1$, which can be understood by observing that the roots of the two Bessel functions do not coincide. Therefore there are singularities in $\mathscr{J}_1$ due to $J_1$. The first discontinuity occurs at $x_c$ and can be stated as

$$\mathscr{J}_1(x_c^-) = -\infty \quad \text{and} \quad \mathscr{J}_1(x_c^+) = +\infty. \tag{22}$$

Using two of the recurrence relations for Bessel functions of the first kind, the first derivative of $\mathscr{J}_1$ can be shown to be

$$\frac{\mathrm{d}}{\mathrm{d}x}[\mathscr{J}_1(x)] = 2\frac{J_0(x)}{J_1(x)} - x\left(1 + \frac{J_0(x)^2}{J_1(x)^2}\right). \tag{23}$$

From Eqs. (22) and (23) it is evident that a discontinuity in the derivative also exists, which can be stated as

$$\frac{\mathrm{d}}{\mathrm{d}x}[\mathscr{J}_1(x_c^-)] = -\infty. \tag{24}$$

The significance of this result, related to an actual rod, is discussed later in the paper. A comparison between the exact Onoe function and the expansion series at various levels of approximation is shown in Fig. 3.

Retaining the first two terms of the Onoe expansion yields the first-order approximation, which, as with the zero-order approximation, is described by a monic polynomial. The solution is given by

$$\gamma^2 = \frac{\rho\omega^2(8(\mu+\lambda) - \rho a^2\omega^2)}{\rho a^2\omega^2(2\mu+\lambda) - 8\mu(2\mu+3\lambda)}. \tag{25}$$

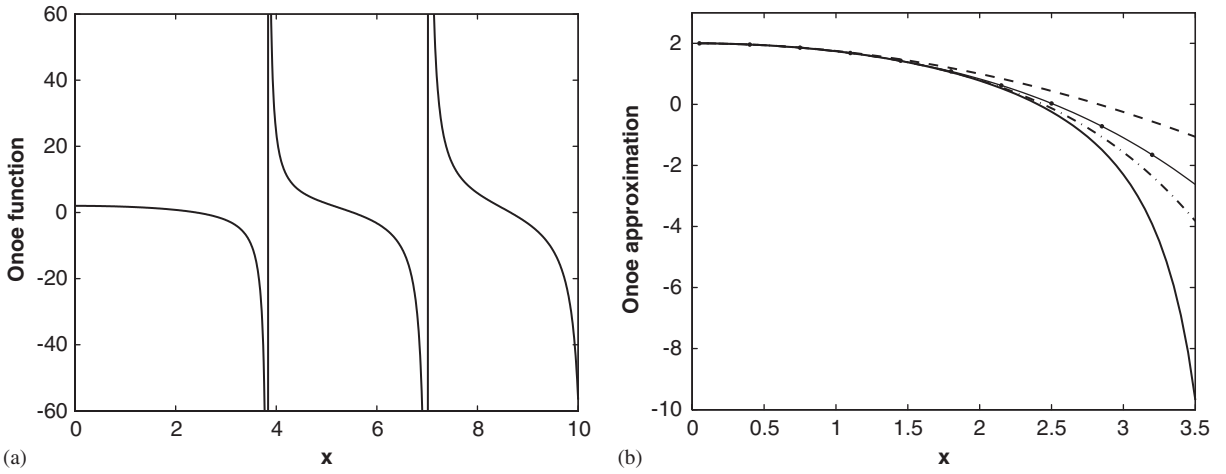


Fig. 3. (a) The Onoe function; and (b) its various orders of approximation given by Eq. (21). (First-order, dashed line; second-order, solid line with dot markers; third-order, dash-dot line; exact function, solid line.)

Similarly, retaining the first three terms of the expansion yields the second-order approximation, which is given by

$$C_1\gamma^6 + C_2\gamma^4 + C_3\gamma^2 + C_4 = 0, \tag{26}$$

where

$$C_1 = 4a^6\mu(\mu+\lambda)(2\mu+\lambda),$$

$$C_2 = \rho a^6\omega^2(8\mu^2 + 12\mu\lambda + 3\lambda^2),$$

$$C_3 = 2a^2(\rho^2a^4\omega^4\lambda - 12\rho a^2\omega^2(2\mu+\lambda)^2 + 96\mu(2\mu+\lambda)(2\mu+3\lambda)),$$

$$C_4 = 192\rho a^2\omega^2(2\mu+\lambda)(\mu+\lambda) - 24\rho^2a^4\omega^4(2\mu+\lambda) - \rho^3a^6\omega^6.$$

The first four terms of the expansion gives the following third-order approximation:

$$C_1\gamma^8 + C_2\gamma^6 + C_3\gamma^4 + C_4\gamma^2 + C_5 = 0, \tag{27}$$

where

$$C_1 = 8a^8\mu(\mu+\lambda)(2\mu+\lambda)^2,$$

$$C_2 = a^6(2\mu+\lambda)(\rho a^2\omega^2(32\mu^2 + 44\mu\lambda + 11\lambda^2) + 64\mu(\mu+\lambda)(2\mu+\lambda)),$$

$$C_3 = \rho a^6\omega^2(\rho a^2\omega^2(40\mu^2 + 72\mu\lambda + 33\lambda^2 + 4\lambda^3/\mu) + 16(2\mu+\lambda)(8\mu^2 + 12\mu\lambda + 3\lambda^2)),$$

$$C_4 = a^2(\rho^3a^6\omega^6(6\mu + 13\lambda + 4\lambda^2/\mu) + 32\rho^2a^4\omega^4\lambda(2\mu+\lambda) - 384\rho a^2\omega^2(2\mu+\lambda)^3 + 3072\mu(2\mu+\lambda)^2(2\mu+3\lambda)),$$

$$C_5 = \rho a^2\omega^2(384(2\mu+\lambda)^2(8(\mu+\lambda) - \rho a^2\omega^2) - 16\rho^2a^4\omega^4(2\mu+\lambda) - \rho^3a^6\omega^6).$$

### 2.6. Determining the complex elastic modulus

Rewriting $\mu$ and $\lambda$ in terms of $E$ and $v$ using Eq. (10), and assuming knowledge of $\gamma$ and $v$, all the approximate rod equations can be rearranged to give directly solvable polynomials in terms of $E$. $\gamma$ can be determined experimentally by taking strain measurements at different positions along a bar with a travelling stress pulse [5]. If $v$ is not known a priori it can also be determined experimentally by simultaneously taking axial and circumferential strain measurements at the same point on the bar [16].

For all the rearranged equations the order of the polynomial is unchanged except the first-order Pochhammer approximation which turns out to be quadratic. For the polynomials of order greater than one there obviously exists multiple roots to the equation, only one of which is the correct solution. However, each root is capable of yeilding the correct modulus if its corresponding propagation coefficient is used. Using the two-mode equation as an example, if the correct modulus is given by the first root when $\gamma = \gamma_1$ is the dominant propagation coefficient, say, then the second root will yield the correct modulus with the second mode propagation coefficient $\gamma_2$. Since $\gamma$ is determined experimentally it is essentially equal to the dominant

propagation coefficient, and therefore the correct modulus is easily identified as the only root that is non-zero at zero frequency. This is because the additional propagating modes only appear at higher frequencies.

## 3. Comparison of rod equations

### 3.1. Deformation mode approximations

Fig. 4 compares the dispersion curves and phase velocities, defined as $c = \omega/k$, for a typical 100 mm diameter aluminium rod ($E = 70\,\text{GPa}$, $\nu = 0.3$, $\rho = 2700\,\text{kg/m}^3$) using the exact Pochhammer equation and four rod approximations; Love, two-mode, three-mode and four-mode. The elementary theory does not exhibit any dispersion (i.e., constant phase velocity) and has not been shown. The Love theory is relatively accurate at lower frequencies due to the inclusion of lateral energy effects, however it diverges at higher frequencies since it does not take into account cross-section warping and therefore shear stress [4]. For the multimode equations it can be seen that as the number of modes increases the error when compared to the exact Pochhammer equation reduces. The four-mode rod equation is surprisingly accurate up to the plotted frequency of 100 kHz, which is above the highest frequency encountered in most impact experiments. It is not entirely clear from the figure, however the phase velocity of the two-mode equation tends towards the exact limiting value equal to the Raleigh phase speed. This results from the value of an adjustable parameter in the rod equation that is usually chosen to provide better agreement with the exact solution [6]. For this reason the two-mode equation provides a better phase velocity approximation at increasingly higher frequencies.

With little difference between the accuracies of the four-mode and Pochhammer equations, the clear advantage of using the four-mode equation is that its solution can be computed directly,

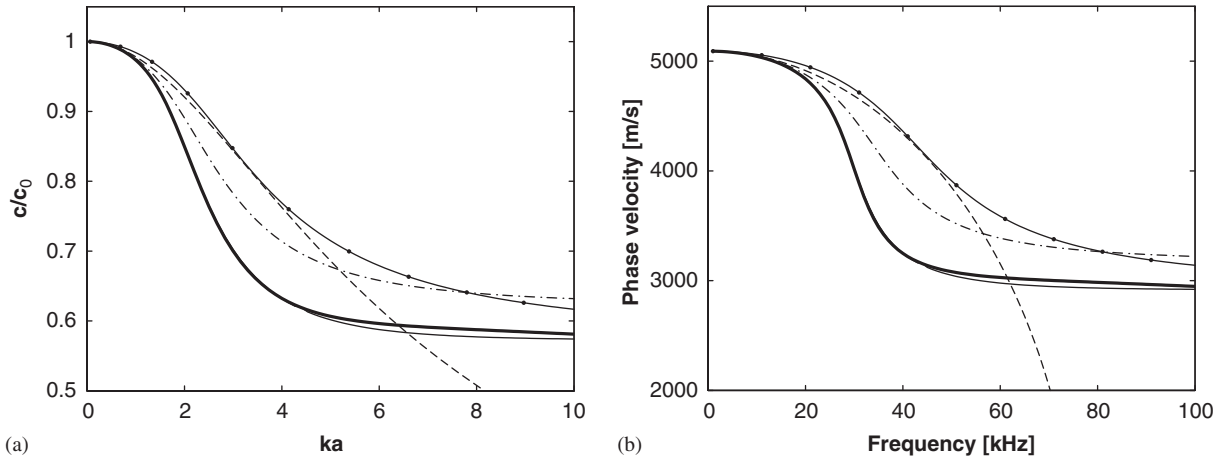


Fig. 4. (a) Dispersion curves for an aluminium bar; and (b) phase velocities for a 100 mm diameter aluminium bar determined using the deformation mode approximation rod equations. (Love, dashed line; two-mode, solid line with dot markers; three-mode, dash-dot line; four-mode, thick solid line; Pochhammer, thin solid line.)

whereas the Pochhammer equation requires an iterative scheme. Computing the four-mode solution was found to be more than 2300 times faster than the Pochhammer solution and less than six times slower than the elementary solution when using 200 data points. Another disadvantage of using the Pochhammer equation is that at any given frequency Eq. (16) has an infinite number of roots. Moreover, as the frequency increases there are additional non-trivial imaginary roots corresponding to new propagating modes. In such cases where multiple roots exist, the actual root obtained is highly dependent on the initial guess of the iterative scheme. Thus, a small increase in frequency may result in the solution 'jumping' to a different propagating mode. Infact, in computing the solutions to the Pochhammer equation, the only initial guess that led to the first mode solution for the complete plotted spectrum was the propagation coefficient from the four-mode equation.

Another advantage is that since these higher-order equations were developed from approximate two-dimensional displacement fields through the cross-section of the rod, similar equations can be developed for a small number of other cross-sectional shapes, for which the Pochhammer equation no longer applies, provided the deformation plane can be approximated as two-dimensional. Practical examples include an annular cross-section, which is another axisymmetrical problem, and a rectangular cross-section with one of the dimensions dominant. Doyle [17] presented, respectively, the quadratic and cubic characteristic equations for the two- and three-mode rod equations for a deep rectangular rod.

### 3.2. Pochhammer approximations

Fig. 5 compares the Pochhammer approximations for the same aluminium rod. The fourth-order approximation, produced to extend the comparison range, was obtained by substituting the first five terms of the Onoe expansion into Eq. (17) and solving using an iterative procedure. Comparing Figs. 4 and 5 it is clear that both the first- and second-order approximations are more

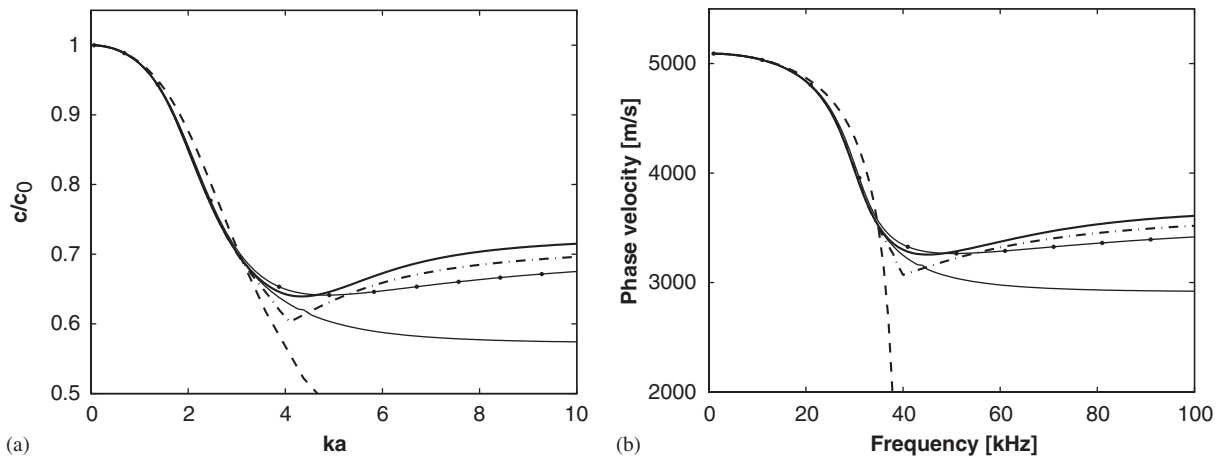


Fig. 5. (a) Dispersion curves for an aluminium bar; and (b) phase velocities for a 100 mm diameter aluminium bar determined using the Pochhammer approximation rod equations. (First-order, dashed line; second-order, solid line with dot markers; third-order, dash-dot line; fourth-order, thick solid line; Pochhammer, thin solid line.)

accurate in the early part of the spectrum than the three-mode equation. This is surprising since the first-order approximation involves a monic polynomial whereas the three-mode equation requires solving the higher-order cubic polynomial.

An interesting observation is that increasing from the second to the third and then the fourth approximation order only marginally improves on the estimate of the phase velocity up to about 38 kHz in comparison to the exact value. However, after around 55 kHz the order of accuracy is reversed and the rod approximations become progressively less accurate. This can be understood by considering Fig. 3. Prior to the first discontinuity at $x_c$, the higher the order of the expansion series, the more accurate the Onoe approximation. After $x_c$ the converse is true, which is why the lower-order approximations become more accurate than higher-order ones.

### 3.3. Pochhammer equation

Another point worth making regards the discontinuity in $\mathscr{J}_1$. Fig. 6 shows the variation of all the arguments of the Onoe function in Eq. (17) with frequency for the same aluminium rod. Since the Pochhammer equation has to be solved for real and imaginary parts, the function typically has four arguments. However, for this particular rod $\mathrm{Re}(\alpha a) = 0$, leaving only three arguments to study. The first argument to cross the first discontinuity of $x_c$ is $x = \mathrm{Im}(\alpha a)$. This has been circled in the figure and occurs at a frequency of 45 kHz. This leads to a numerical inaccuracy when attempting to solve for the imaginary part of Eq. (17) that corresponds to the wavenumber. The

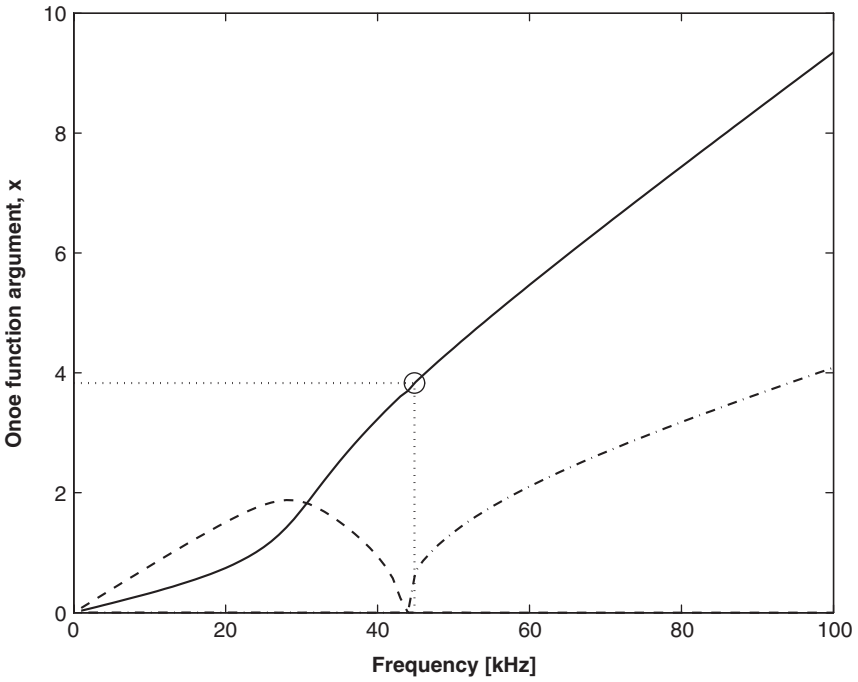


Fig. 6. Argument of the Onoe function against frequency for a 100 mm diameter aluminium bar. ($x = \mathrm{Im}(\alpha a)$, solid line; $x = \mathrm{Re}(\beta a)$, dashed line; $x = \mathrm{Im}(\beta a)$, dash-dot line.)

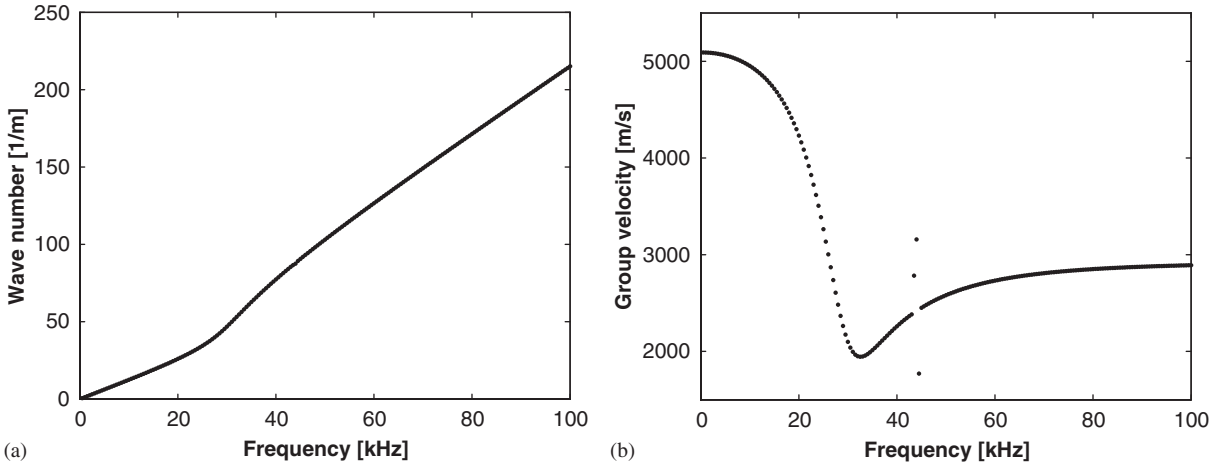


Fig. 7. (a) Wavenumber; and (b) group velocity for a 100 mm diameter aluminium bar determined using the Pochhammer equation.

inaccuracy arises due to machine truncation errors, which can be explained with the aid of Eq. (24). The truncated value, while relatively small in magnitude, is magnified in $\mathscr{J}_1$ near the discontinuity since on one side of this point the gradient of the function is $-\infty$.

To demonstrate this Fig. 7 shows the wavenumber and group velocity, defined as $c_g = \mathrm{d}\omega/\mathrm{d}k$, for the aluminium rod that was determined using the Pochhammer equation. At the discontinuity frequency of 45 kHz we would expect an error in the wavenumber, and indeed one is present despite its smooth appearance. The error is evidenced in the group velocity and can be explained due to the ill-conditioned process of differentiation. That is, small perturbations in the data ($k$) lead to large perturbations in the solution ($c_g$). Thus a further limitation, albeit a small one, is placed on the use of the Pochhammer equation when calculation of the group velocity is required. (Note that in the algorithms used to obtain all the Pochhammer solutions, Eq. (16) was used and not Eq. (17).)

Two more discontinuity crossings occur in Fig. 6; the argument $x = \mathrm{Im}(\beta a)$ crosses the first discontinuity at a higher frequency of 94 kHz, and the argument $x = \mathrm{Im}(\alpha a)$ crosses the second discontinuity, which can be observed from Fig. 2 to occur at $x \approx 7.01$, at a frequency of 75 kHz. However, numerical errors are not clearly present at these frequencies in Fig. 7(b). This is because the terms preceding the Onoe functions in Eq. (17) increase their dominance at higher frequencies, such that

$$4\gamma^2\alpha^2 > 10^9 \mathscr{J}_1(\beta a) \quad \text{at } 94\,\text{kHz},$$

$$(\beta^2 + \gamma^2)^2 > 10^8 \mathscr{J}_1(\alpha a) \quad \text{at } 75\,\text{kHz}.$$

### 3.4. Elastic modulus results

Fig. 8 shows the computed elastic modulus for the same aluminium rod using the approximate rod equations with the exact propagation coefficient that was obtained from the Pochhammer

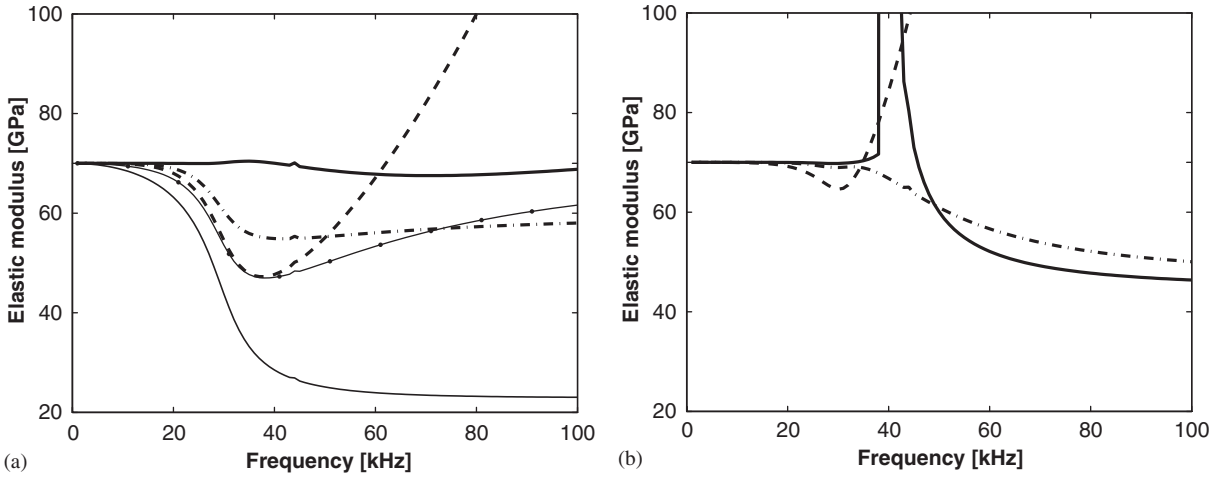


Fig. 8. Elastic modulus of an aluminium bar determined using the exact propagation coefficient obtained from the Pochhammer equation with (a) the deformation mode approximation equations (elementary, thin solid line; Love, dashed line; two-mode, solid line with dot markers; three-mode, dash-dot line; four-mode, thick solid line); and (b) the Pochhammer approximation equations (first-order, dashed line; second-order, dash-dot line; third-order, solid line).

equation. Compared to the phase velocities, significant errors occur in the elastic modulus at an earlier position in the spectrum. Considering Fig. 8(a) first, the Love theory provides a slightly better approximation in the early part of the spectrum than the two-mode equation. As would be expected, as the number of deformation modes increases, the accuracy of the computed modulus improves. The four-mode equation is very close to the true modulus of 70 GPa for the whole plotted spectrum. From Fig. 8(b) the first-order approximation provides a very good estimate for the modulus at low frequencies, again being more accurate than both the two- and three-mode equations, however it rapidly becomes inaccurate with increasing frequency. The third-order approximation exhibits large inaccuracies at a frequency of 40 kHz. This inaccuracy can also be observed in Fig. 5 as a kink in the dispersion and phase velocity curves. Similar inaccuracies are present in the first-order approximation (although not as pronounced) and higher odd-order approximations, however their origin is not clear. Also worth noting is the numerical error present in all the curves at a frequency of 45 kHz, which arises from the previously mentioned error in a propagation coefficient computed from the Pochhammer equation.

## 4. Conclusions

Several rod equations for longitudinal wave propagation have been compared. A newly presented four-mode equation, based on lower-order rod approximations, has been shown to provide extremely good agreement with the exact stress wave propagation as described by the Pochhammer–Chree equation. The four-mode equation has the advantage of a direct solution procedure, allowing much faster computation than iteratively solving the Pochhammer equation. It can also be derived for other two-dimensional cross-sections other than the circular bar.

Three approximations based on the Pochhammer equation were also presented. The first-order Pochhammer approximation, while only a monic polynomial in $\gamma^2$, is very accurate for longer wavelengths in the spectrum. Compared to the other monic polynomials discussed here, namely, the elementary and Love theories, the first-order Pochhammer approximation appears far better. Surprisingly, it is also more accurate than both the two- and three-mode equations for low-frequencies waves. The only limitation is its sole applicability to circular bars.

Selecting the rod equation to use for a certain level of solution accuracy can be first categorised into the likely magnitude of the non-dimensional parameter *ka*, and then into the ease of the solution procedure. For relatively small values of *ka* the first-order Pochhammer approximation is very simple and accurate. For large values of *ka* the two-mode equation, which is solved using the well-known quadratic formula, is not sufficiently accurate. As there is little difference in the complexity of the cubic and quartic formulas, there is no advantage in using the three-mode equation. Since the accuracy of the four-mode equation is comparable to Pochhammer equation, it is clearly the best choice rod approximation equation.

## References

[1] H. Kolsky, *Stress Waves in Solids*, Dover, New York, 1963.
[2] H. Zhao, G. Gary, On the use of a viscoelastic split Hopkinson pressure bar, *International Journal of Impact Engineering* 19 (1997) 319–330.
[3] R.M. Davies, A critical study of the Hopkinson pressure bar, *Philosophical Transactions of the Royal Society* 240 (1948) 375–457.
[4] W.A. Green, Dispersion relations for elastic waves in bars, in: I.N. Sneddon (Ed.), *Progress in Solid Mechanics*, vol. 1, North–Holland, Amsterdam, 1960, pp. 225–261.
[5] C. Bacon, An experimental method for considering dispersion and attenuation in a viscoelastic Hopkinson bar, *Experimental Mechanics* 38 (1998) 242–249.
[6] K.F. Graff, *Wave Motion in Elastic Solids*, Dover, New York, 1991.
[7] W. Magnus, F. Oberhettinger, R.P. Soni, *Formulas and Theorems for the Special Functions of Mathematical Physics*, third ed., Springer, New York, 1966.
[8] R.D. Mindlin, H.D. McNiven, Axially symmetric waves in elastic rods, *ASME Journal of Applied Mechanics* 27 (1960) 145–151.
[9] R.D. Mindlin, G. Herrmann, A one-dimensional theory of compressional waves in an elastic rod, in: *Proceedings of the First US National Congress of Applied Mechanics*, 1950, pp. 187–191.
[10] C.B. Boyer, U.C. Merzbach, *A History of Mathematics*, second ed., Wiley, Singapore, 1989.
[11] A.E.H. Love, *A Treatise on the Mathematical Theory of Elasticity*, fourth ed., Cambridge University Press, Cambridge, 1927.
[12] M. Abramowitz, I.A. Stegun, *Handbook of Mathematical Functions with Formulas, Graphs, and Mathematical Tables*, ninth ed., Dover, New York, 1972.
[13] H. Zhao, G. Gary, A three-dimensional analytical solution of the longitudinal wave propagation in an infinite linear viscoelastic cylindrical bar. Application to experimental techniques, *Journal of the Mechanics and Physics of Solids* 43 (1995) 1335–1348.
[14] M. Onoe, H.D. McNiven, R.D. Mindlin, Dispersion of axially symmetric waves in elastic rods, *ASME Applied Mechanics* 29 (1962) 729–734.
[15] M. Onoe, *Tables of Modified Quotients of Bessel Functions of the First Kind for Real and Imaginary Arguments*, Columbia University Press, New York, 1958.
[16] A. Benatar, D. Rittel, A.L. Yarin, Theoretical and experimental analysis of longitudinal wave propagation in cylindrical viscoelastic rods, *Journal of the Mechanics and Physics of Solids* 51 (2003) 1413–1431.
[17] J.F. Doyle, *Wave Propagation in Structures*, second ed., Springer, New York, 1997.